Geol. Mag. **154** (*5*), *2017, pp. 983–1000.* © *Cambridge University Press 2016*
doi:10.1017/S0016756816000558

Structural and kinematic analyses of the basement window within the hinterland fold-and-thrust belt of the Zagros orogen, Iran

KHALIL SARKARINEJAD* & SOMAYE DERIKVAND

Department of Earth Sciences, College of Sciences, Shiraz University, Shiraz 71454, Iran

(*Received* 1 December 2015; *accepted* 18 May 2016; *first published online* 4 November 2016)

Abstract – The Zagros hinterland fold-and-thrust belt is located in the central portion of the Zagros Thrust System and consists of the exhumed basement windows associated with NW-striking and NE-dipping flexural duplex structures that contain in-sequence thrusting and related folds. Mylonitic nappes of the basement were exhumed along deep-seated sole thrusts of the Zagros Thrust System. Lattice preferred orientation (LPO) *c*-axes of quartz show asymmetric type-1 crossed girdles that demonstrate a non-coaxial deformation under plane strain conditions. Based on the opening angles of quartz c-axis fabric skeletons, deformation temperatures vary from 425 ± 50 °C to 540 ± 50 °C, indicating amphibolite facies conditions. The estimated mean kinematic vorticity evaluated from quartz c-axis of the quartzo-feldspathic mylonites ($W_m = 0.55 \pm 0.06$) indicates the degree of non-coaxiality during mylonite exhumation. The estimated angle θ between the maximum instantaneous strain axis (ISA_1) and the transpressional zone boundary is 17°, and the angle of oblique convergence is 57° in the M_2 nappe of the basement involved. This indicates that the mylonitic nappe was formed by a combination of 62 % pure shear and 38 % simple shear during oblique convergence.

Keywords: transpressional zone, mylonitic nappe, vorticity, quartz c-axis, Zagros orogenic belt.

1. Introduction

Transpressional shear zones are common deformational features in many tectonic settings that accommodate significant amounts of strain across oblique convergent plate boundaries. During oblique convergence, lithospheric plates undergo shortening and transpressional deformation (Sanderson & Marchini, 1984; Tikoff & Teyssier, 1994) which are associated with a wide orogenic belt. The tectonic transport vector is an effective parameter to specify the geometry and kinematics of deformation (Elliott, 1983). Inclined transpression was defined by Jones *et al.* (2004) as isochronous contractional and dip-slip shearing that is a non-coaxial and non-plane strain deformation. An example of the classical crustal inclined transpression zone is the Zagros Thrust System, which involves ductile transpressional deformation (Mohajjel & Fergusson, 2000; Sarkarinejad, 2007; Sarkarinejad & Azizi, 2008; Sarkarinejad, Faghih & Grasemann, 2008; Sarkarinejad *et al.* 2012; Sarkarinejad & Ghanbarian, 2014) resulting from relative motion between the Afro-Arabian continent and the Iranian microcontinent. Structural and kinematic analyses of the transpressional deformation indicate exhumation of the highly strained mylonitic shear zones associated with the nappes of the basement involved in the recently recognized hinterland fold-and-thrust belt of the Zagros orogen (Sarkarinejad & Alizadeh, 2009; Sarkarinejad & Ghanbarian, 2014) and improve our understanding of strain partitioning within the still active zone of inclined transpression in the Zagros Mountains.

Analyses of lattice preferred orientation (LPO) patterns of quartz *c*-axes and of vorticity are important techniques for investigating the kinematics and geometry of flow in shear zones. The first vorticity analysis in deformed mylonites from the French Pyrenees (Passchier, 1987) marked important progress in developing methods for quantifying vorticity and has been applied since by many geologists (e.g. Passchier & Urai, 1988; Wallis, 1992; Simpson & De Paor, 1993; Tikoff & Fossen, 1995; Grasemann, Fritz & Vannay, 1999; Holcombe & Little, 2001; Gomez-Rivas *et al.* 2007; Jessup, Law & Frassi, 2007; Xypolias, 2009). Since then the vorticity of deformed rocks has been analysed using various techniques (Xypolias & Doutsos, 2000; Bailey & Eyster, 2003; Law, Searle & Simpson, 2004; Marques, Schmid & Andersen, 2007; Sarkarinejad, 2007; Iacopini *et al.* 2008; Sarkarinejad & Azizi, 2008; Sullivan, 2008; Frassi *et al.* 2009; Thigpen *et al.* 2010; Sarkarinejad & Ghanbarian, 2014).

Transpression can be divided into pure shear and simple shear dominated using the angle of convergence (Fossen & Tikoff, 1993). Kinematic partitioning of the pure shear and simple shear strain components in spatially separated domains is an important aspect of many transpressional systems (Fossen, Tikoff & Teyssier, 1994; Tikoff & Teyssier, 1994; Jones & Tanner, 1995; Teyssier, Tikoff & Markley, 1995). This paper describes well-exposed structural and microstructural fabrics, quartz c-axis LPOs, finite strain and kinematic vorticity analyses and deformation

*Author for correspondence: sarkarinejad@susc.ac.ir

https://doi.org/10.1017/S0016756816000558 Published online by Cambridge University Press

temperature obtained from the exhumed Zagros basement-involved mylonite nappes.

2. Geological and tectonic setting

The Zagros orogeny resulted from collision between the Afro-Arabian continent and the Iranian microcontinent in the Cretaceous (Alavi, 1994), and this belt is still an active convergent boundary (Allen, Jackson & Walker, 2004; Regard *et al.* 2004; Talebian & Jackson, 2004; Tatar, Hatzfeld & Ghafory-Ashtiyani, 2004; Vernant *et al.* 2004; Authemayou *et al.* 2005) with a convergence rate of 22 ± 2 mm a^{-1} at N8° ± 5° E (Vernant *et al.* 2004). The Zagros suture is the zone along which the Neo-Tethys closed by subduction of the oceanic crust beneath the Iranian microcontinent. This zone marks the boundary between the hinterland fold-and-thrust belt and the foreland fold-and-thrust belt, and is recognizable by the presence of the radiolarian oceanic sediments (Figs 3, 6a, further below), ophiolites and a contrast in P-wave velocities (Vergés *et al.* 2011).

The Zagros orogenic belt can be divided into several structural domains from SW to NE. These include: Zagros foreland folded belt, Zagros foreland fold-and-thrust belt (Stöcklin, 1968; Berberian & King, 1981; Alavi, 1994), Zagros suture zone (Sarkarinejad, 2005), Zagros hinterland fold-and-thrust belt (Sarkarinejad & Ghanbarian, 2014), Sanandaj-Sirjan HP-LT/HT-LP paired metamorphic belts (Sarkarinejad, 1999) and the Urumieh–Dokhtar magmatic belt (Stöcklin, 1968). The study area is located in the basement-involved portion of the Zagros hinterland fold-and-thrust belt and is situated between Doroud and Azna cities NE of Lorestan province in western Iran (Fig. 1). Previous geological maps of the study area (Sahandi *et al.* 2006; Goodarzi, 2010) have been modified and a new geological map has been constructed (Fig. 2). The metamorphic rocks consist of quartzo-feldespathic mylonites, ultramylonites, amphibolitic mylonites, calc-schists, dolomarbles, schists, volcanic rocks, limestones and sandstones, a basal conglomerate and radiolarites. The structures are attributed to three phases of deformation.

Several generations of structures were produced during three phases of deformation. Ptygmatic folds, boudinaged folds, folded boudins, parasitic folds, harmonic and disharmonic folds are common. Interference patterns of superposed folds are observed in the dolomarbles and calc-schists. The area is dominated by imbricate thrust systems and duplex structures which are developed together with fault-related folds (Fig. 6d, further below). Abundant small-scale and map-scale folds are asymmetric and related to thrust systems with a ramp–flat geometry. The main structures on the structural map (Fig. 3) strike mainly NW–SE.

3. Deformation history

The hinterland of the Zagros orogenic belt has undergone three phases of deformation, defined as D_1, D_2 and D_3 (Sarkarinejad & Azizi, 2008). The $^{40}Ar/^{39}Ar$ step heating from the biotite grains of gneiss recorded plateau ages of 119.95 ± 0.88 Ma and 112.58 ± 0.66 Ma (Sarkarinejad, Godin & Faghih, 2009) which occurred during collision between the Afro-Arabian and Iranian microcontinents during D_1 deformation. These late Aptian ages are coincident with forming S_1 foliations, L_1 lineations and F_1 folds at the peak of metamorphism.

$^{40}Ar/^{39}Ar$ step heating of the hornblende of the amphibolites estimated ages of 89.09 ± 1.34 Ma and 90.18 ± 1.88 Ma, which indicate that S_2 foliations, L_2 stretching lineations and F_2 folds formed during the Turonian–Cenomanian (Sarkarinejad, Godin & Faghih, 2009). This phase (D_2) of deformation is characterized by obduction of ophiolites over the toe wedge of the hinterland, exhumation of the high-pressure metamorphic rocks and inversion of the half-grabens formed in the mid-Permian–Triassic (Stampfli *et al.* 2001) to contractional regime along the Zagros accretionary prism.

Exhumation of mylonitic nappes by basement-involved shear zones, fault-related folds and formation of S/C shear band cleavages (Sarkarinejad, 2007; Sarkarinejad & Azizi, 2008) by the latest phase (D_3) of deformation.

4. Outcrop scale structures

4.a. Foliations

The metamorphic rocks of the area exhibit penetrative foliations S_1 and S_2. S_1 foliations display a well-developed cleavage in muscovite schists. The S_1 foliation mean orientation is N59° W, 37° NE (Fig. 4a). S_1 foliations are overprinted by the second generation of foliations trending NW–SE that commonly lie at an angle of about 20° to S_1 (Fig. 4b). S_2 foliation formed in a lower-grade condition S_1 forming the asymmetric crenulation cleavages and meso- and micro-folding (Fig. 8f, further below). Mean orientation of S_2 is N40° W, 46° NE (Fig. 4b). S/C shear band cleavages were developed along the shear zones during a third phase of deformation (D_3).

4.b. Stretching lineation

L_1 stretching lineation is well developed by the long axes of feldspar and amphibole minerals, thin quartz ribbons and mica fishes in schists. A second type of stretching lineation is defined by mesoscopic fold hinge lines. The mean plunge and trend of L_1 is 41°, N38° E and the mean orientation of L_2 is 48°, N45° E (Fig. 4c, d).

4.c. Superposed folds

Many mesoscopic superposed folds are well developed in dolomarble and calc-schist in the western part of the study area. Superposed folds form type-2 and type-3 (Fig. 7e, f, further below) interference patterns (Ramsay, 1967). These interference patterns resulted from overprinting of F_1 and

https://doi.org/10.1017/S0016756816000558 Published online by Cambridge University Press

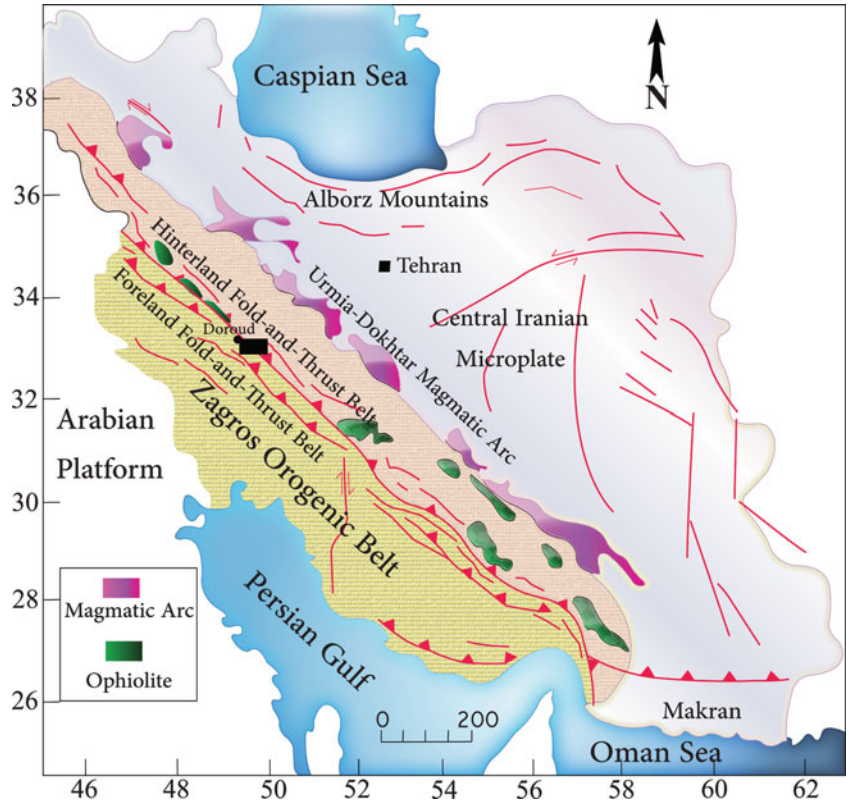

Figure 1. (Colour online) Structural domains of the Zagros orogenic belt in western Iran (Sarkarinejad & Ghanbarian, 2014). Black inset rectangle shows location of the Doroud–Azna region of the Zagros hinterland fold-and-thrust belt.

F_2 folds. Figure 7f (further below) illustrates a superposed fold with type-2 interference pattern that was produced when an F_2 fold affected the axial surface of an F_1 fold (Ramsay 1962; Ramsay & Huber, 1987, p. 492). Overprinting by D_3 deformation on both previous deformations resulted in complex folding locally.

4.d. Boudins

Asymmetrical boudins and pinch-and-swell structures are abundant in the study area. There are boudins of quartz veins, chert bands and dolomitic layers enveloped by less competent layers of marble and muscovite schists. Some of the boudins are strongly sheared and imbricated to form piggyback structures (Fig. 7a, further below). F_1 boudins in the cores of F_2 folds documented polyphase of deformation (Fig. 7c, further below). The quartz and dolomitic layers commonly form domino, rotated shear band and drawn boudins (Goscombe, Passcier & Hand, 2004), within schist and phyllonitic fold limbs. Thin layers of quartz in the marble and dolomite are folded and boudinaged parallel to S_2. Most of the asymmetrical boudins indicate a dextral sense of shear.

5. Thrust-and-fold structures

Thrust sheets, duplexes and imbricate thrust systems involving fault-bend folds are widespread in this area. Most of the map-scale hinterland dipping thrusts that crop out in the Doroud–Azna region are consistent with the NW-trending Zagros Thrust System. A cross-section of these thrusts is presented further below in Figure 12. Thrusting throughout the area has formed imbricated stacks that strike NW and dip NE with a mean orientation N38° W, 44° NE (Fig. 5). Younger layers in the hanging wall are juxtaposed against older layers in the footwall. Fault-bend folds develop by movement over thrust ramps (Suppe, 1983), and abundant mesoscopic fault-bend folds are observed in the metamorphic rocks that confirm the general kinematics of fault-related folds (e.g. Fig. 6b). Duplex structures in the Permian calc-schists locally overlap overturned folds to create antiformal stacks (Fig. 6e). Some NE-striking faults with a strike-slip component occur in the study area; these transfer faults have a mean orientation of N41° E, 67° NW (Fig. 5).

6. Shear zone structures

Widespread shear zones are exposed along the flexural-slip duplexes and imbricate stacks in the hinterland of the Zagros Thrust System. Two shear zones within the basement are recognized in the Doroud–Azna region. These shear zones are named M_1 and M_2 (Fig. 12, further below) and formed in the D_3 deformation phase. They are recognized by the juxtaposition of basement inliers. The M_1-shear zone exposes amphibolitic mylonite, and the M_2-shear zone exposes quartzo-feldspathic mylonite. These mylonites are overlain by

https://doi.org/10.1017/S0016756816000558 Published online by Cambridge University Press

https://doi.org/10.1017/S0016756816000558 Published online by Cambridge University Press

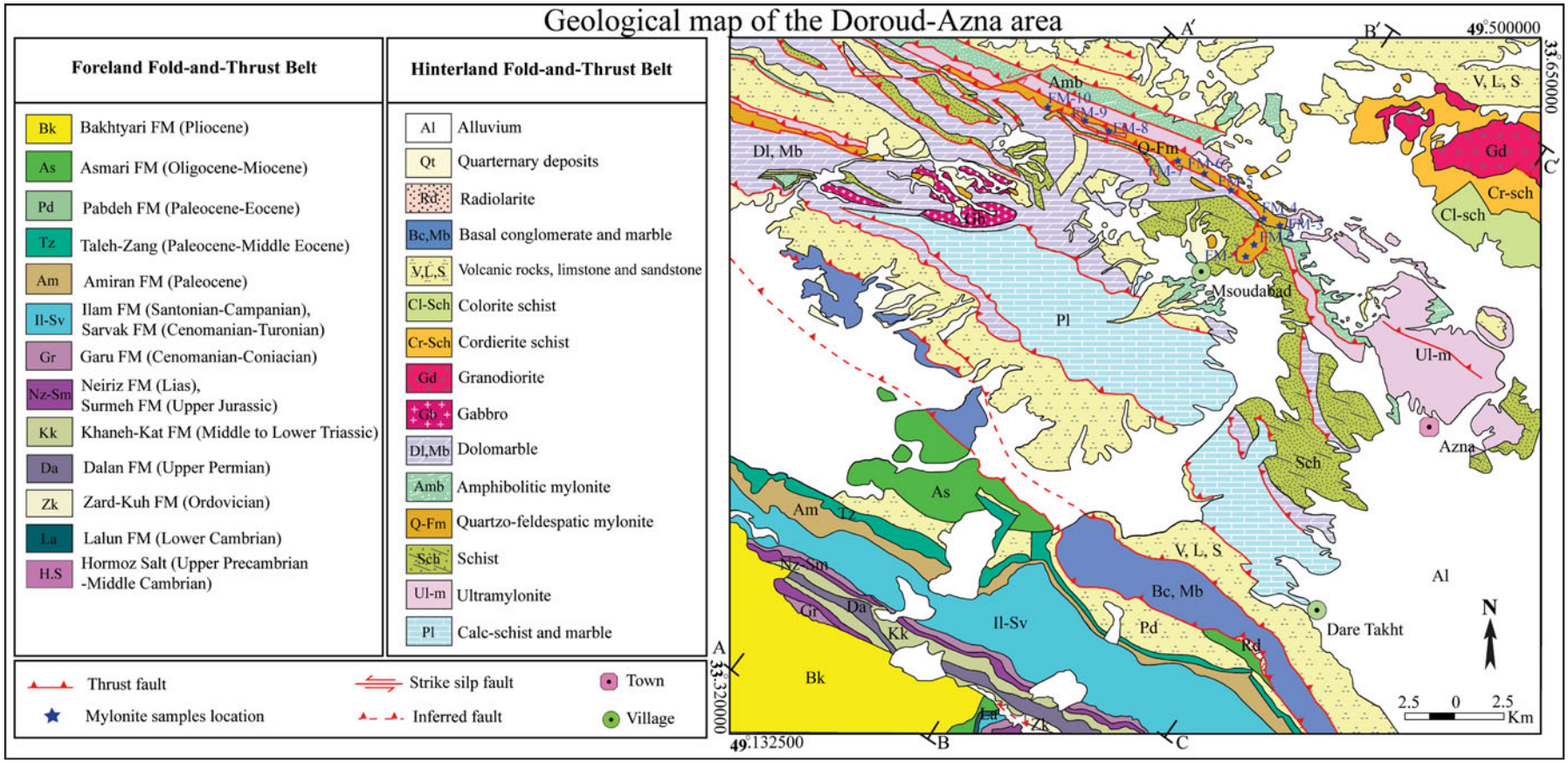

Figure 2. (Colour online) Detailed geological map of the Doroud–Azna area.

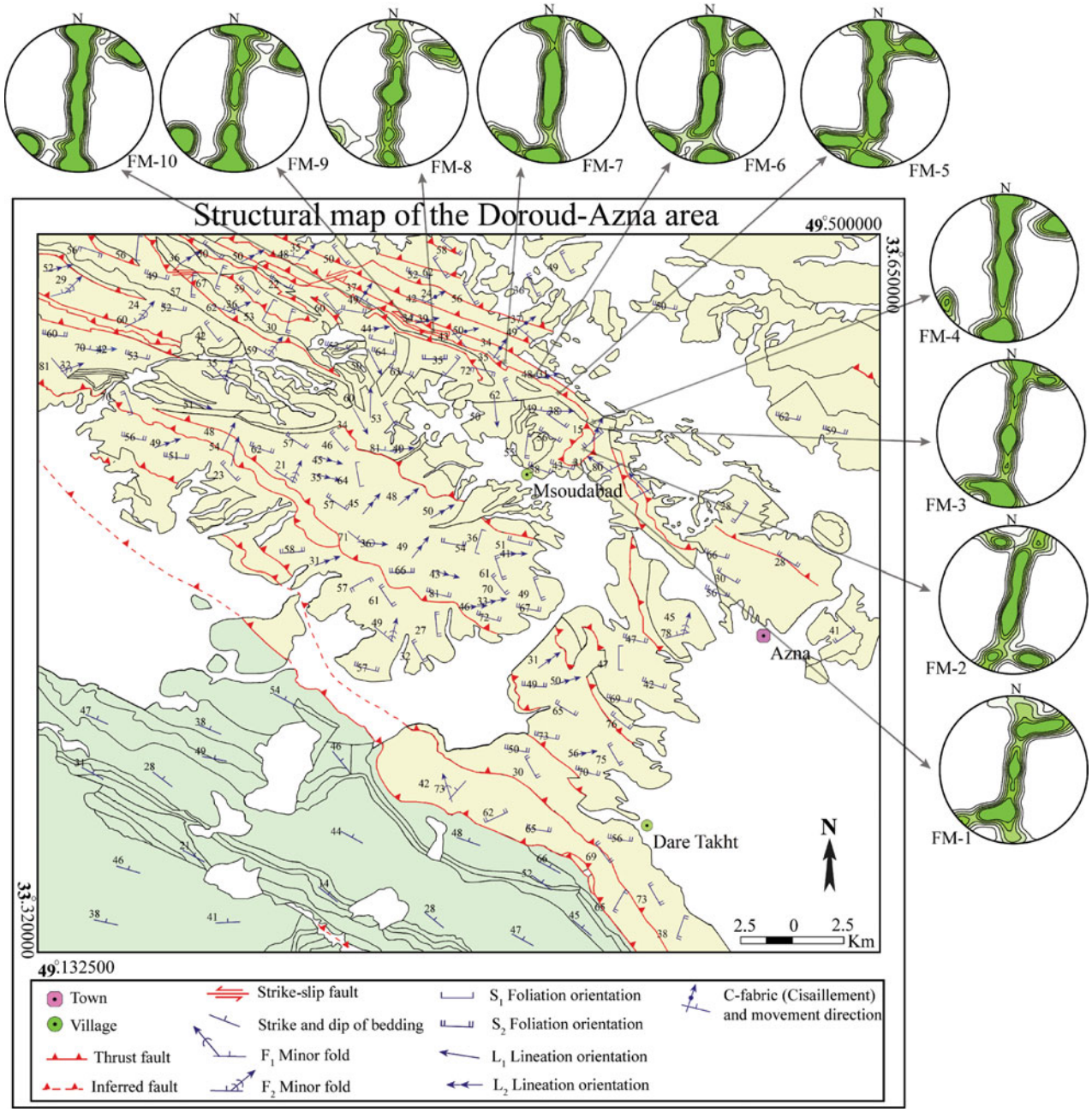

Figure 3. (Colour online) Structural map of the Doroud–Azna area. The Zagros hinterland fold-and-thrust belt is shown in a cream colour, and the Zagros foreland fold-and-thrust belt in the SW corner is shown in green. With respect to the locality of the samples, stereographic projections of the quartz c-axis fabrics are shown on the map.

volcanic rocks, limestone, sandstone, muscovite schist, calc-schist and dolomarble with ages from Middle Triassic to Middle Cretaceous that folded by fault-bend folding. In some areas mylonites are folded and overridden by thrusts (Fig. 6c). NE-dipping shear zones are *c.* 17 km long and 1 km wide. Asymmetrical σ-type and δ-type porphyroclast systems with lengths up to 1 cm within the shear zones indicate top-to-the-SE sense of shear. The recrystallized quartz in quartzo-feldspathic mylonites displays a well-developed c-axis LPO. Cross-sections, temperature and pressure conditions of the formation of mylonites, overall deformation style and high-strain structures all indicate that the shear zones are deeply rooted. Indeed, M_1 and M_2 shear zones are exhumed slices of the basement in the study area. Figure 7d shows a polished slab of the quartzo-feldspathic mylonite in the XZ-plane (parallel to the stretching lineation and perpendicular to foliation) as situated in the M_2 shear zone. Asymmetrical porphyroclasts of feldspar are surrounded by dynamically recrystallized quartz and fine-grained muscovite. Porphyroclasts commonly have an internal monoclinic shape (Passchier & Simpson, 1986). Mesoscopic S/C shear band cleavages in the XZ-plane are related to the third phase of deformation (D_3). The S/C shear band cleavages indicate a dextral sense of shear, consistent with the complete Zagros Thrust System.

https://doi.org/10.1017/S0016756816000558 Published online by Cambridge University Press

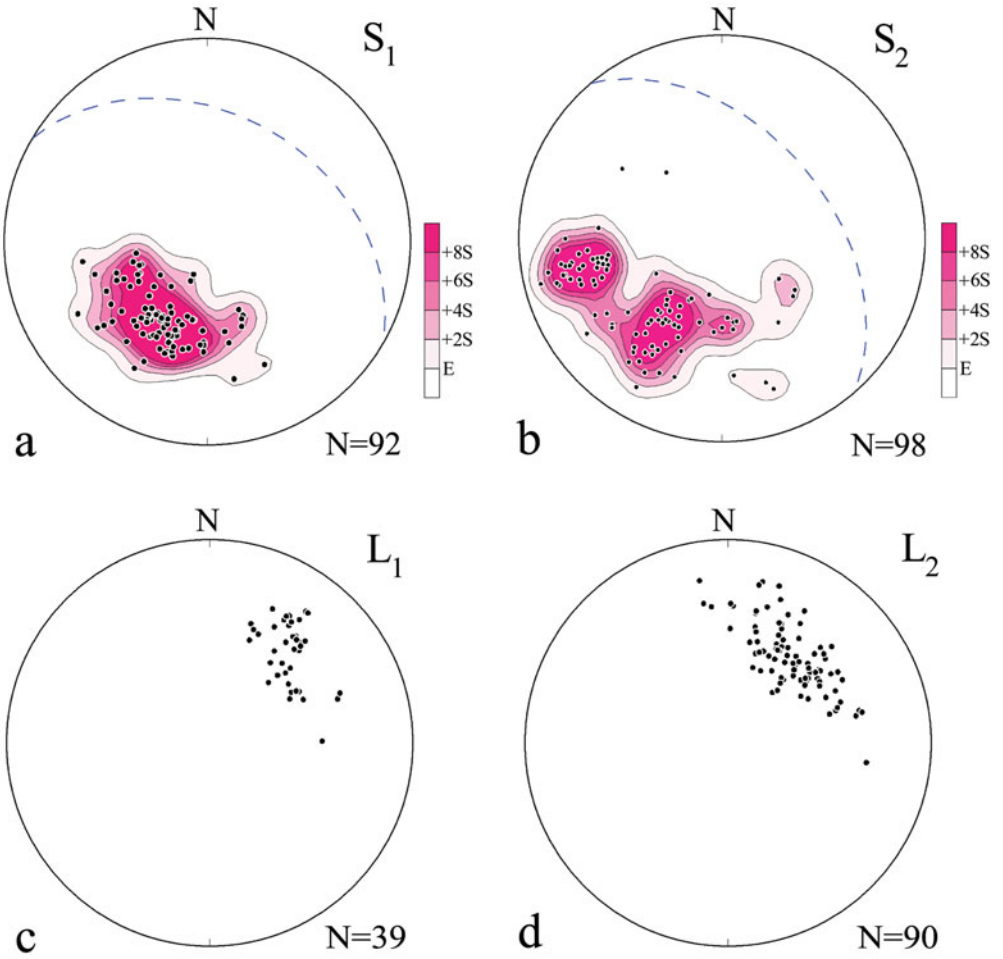

Figure 4. (Colour online) Lower-hemisphere, equal-area stereographic projections of poles to the foliations (S_1 and S_2) and lineations (L_1 and L_2) developed during D_1 and D_2 deformation events. They are contoured at 1 %, 2 %, 4 %, 6 % and 8 % per 1 % area. (a) Poles to S_1 foliation and mean orientation plane. (b) Poles to S_2 foliation and mean orientation plane. (c) L_1 lineations, related to the D_1 deformation event. (d) L_2 lineations, related to the D_2 deformation event.

7. Shear sense indicators

The sense of shear in deformed rocks can be deduced by mesoscopic and microscopic structures (Simpson & Schmid, 1983; Law, 1990; Passchier & Trouw, 2005). These structures are studied in planes parallel to the stretching lineation and perpendicular to the foliation. All of the investigated shear sense indicators, including sheared boudins (Fig. 7a), S/C fabrics (Figs 7b, 8a), porphyroclasts (Fig. 8c, d), mica fishes, shear bands (Fig. 8e), bookshelf structures (Fig. 8b) and asymmetrical folds, show a top-to-the-SE sense of shear in this area.

7.a. σ-, δ-type porphyroclasts

Rotated porphyroclasts wrapped by a fine-grained recrystallized matrix are produced predominantly during high-grade ductile deformation with monoclinic symmetry (Passchier & Trouw, 2005). Porphyroclasts of K-feldspar and hornblende are observed in the quartzo-feldspathic mylonite and amphibolitic mylonite, respectively. K-feldspar porphyroclasts are embedded in a recrystallized fine-grained K-feldspar and quartz (Fig. 8c), and occasionally the K-feldspar porphyroclasts are mantled by recrystallized fine-grained K-feldspar, quartz and biotite. Fine recrystallized K-feldspar and quartz grains indicate medium to high-grade deformation conditions. The samples of amphibolitic mylonite with asymmetric hornblende grains show that hornblende was stable during deformation (Fig. 8d).

7.b. S/C shear bands

Shear band cleavages in mylonite and schist are characterized by C- and S-planes. The C-plane is parallel to the shear zone boundaries and is transected by the S-plane (Berthe, Choukroune & Gapais, 1979; Berthe, Choukroune & Jegouzo, 1979; Lister & Snoke, 1984). With respect to the internal and external asymmetry axes, the shear band cleavages indicate a dextral sense of shear (Fig. 8e).

7.c. Bookshelf structures

Bookshelf structures show two sets of micro-faults. Synthetic slip is consistent with regional dextral sense

https://doi.org/10.1017/S0016756816000558 Published online by Cambridge University Press

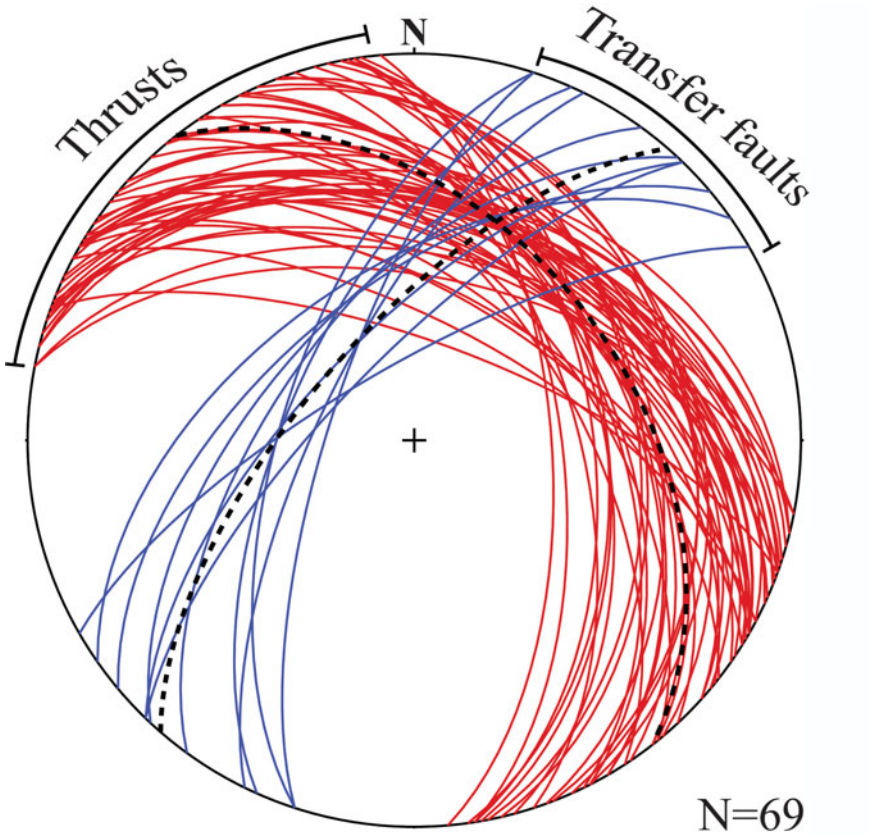

Figure 5. (Colour online) Lower-hemisphere, equal-area stereographic projection of the thrusts (red) and transfer faults (blue).

of shear, and antithetic micro-faults are opposite to the main sense of movement (Fig. 8b). The angle between the micro-faults and the mylonitic foliation is smaller than 45°. Bookshelf sliding is frequently observed between rotated porphyroclasts and can be used as a shear sense indicator.

8. Quartz c-axis fabrics

An important effect of intracrystalline deformation of quartz is the formation of c-axis LPOs that are related to deformation conditions and geometry (Passchier & Trouw, 2005). Quartz c-axes were measured in ten oriented samples of quartzo-feldspathic mylonites from different structural positions along a NE–SW transverse line across the Zagros Thrust System (Fig. 9). The location of the samples is given in Figures 2 and 3. In each sample, c-axis measurements of 400–500 recrystallized grains were made on thin sections perpendicular to foliation and parallel to the stretching lineation, using an optical microscope equipped with a five-axis universal stage. The foliation plane is assumed to be the XY-plane of the finite strain ellipsoid, and the stretching lineation is the x-axis. Fabric skeletons (Fig. 9) show external and internal asymmetries (Law, 1990), indicating a non-coaxial top-to-the-SE sense of shear. They display an obliquity of the central girdle segment with respect to the reference frame (ψ), with values of 60–70°. Also, the fabric asymmetry is determined by the relative magnitudes of angles C_1 and C_2 (external asymmetry) and ω_1 and ω_2 (internal asymmetry) (Law, Knipe & Dayan, 1984; Platt & Behrmann, 1986; Law, 1987, 1990). C-axis fabric skeletons show both external and internal fabric asymmetry ($\psi = 81°$, $\omega_1 = 75°$ and $\omega_2 = 25°$ for FM-1 sample) (Fig. 9; Table 1). The asymmetry of quartz c-axis fabrics relative to the foliation plane indicates non-coaxial progressive deformation. The density distributions of quartz c-axis fabric diagrams obtained from the Doroud–Azna area reveal a pattern of asymmetrical type-1 crossed girdle that shows non-coaxial and plane strain deformation (Etchecopar, 1977; Lister, 1977; Lister, Paterson & Hobbs, 1978; Lister & Paterson, 1979; Etchecopar & Vasseur, 1987; Jessel & Lister, 1990; Law, 1990).

9. Finite strain analysis using R_f/φ method

The R_f/φ method is a powerful graphical analysis technique for calculating the finite strain of deformed elliptical fabrics (Ramsay, 1967; Dunnet, 1969). This method utilizes the mathematical relationship between the sectional orientations and ellipticity of deformed elliptical and spherical objects to calculate the two-dimensional magnitude and orientation of finite strain (Ramsay, 1967; Dunnet, 1969; Ramsay & Huber, 1983, p. 67; Lisle, 1985). The R_f/φ method has been widely used for regional strain analysis. Measurements of aspects ratio (R_f) major and minor axes of ellipsoids were

https://doi.org/10.1017/S0016756816000558 Published online by Cambridge University Press

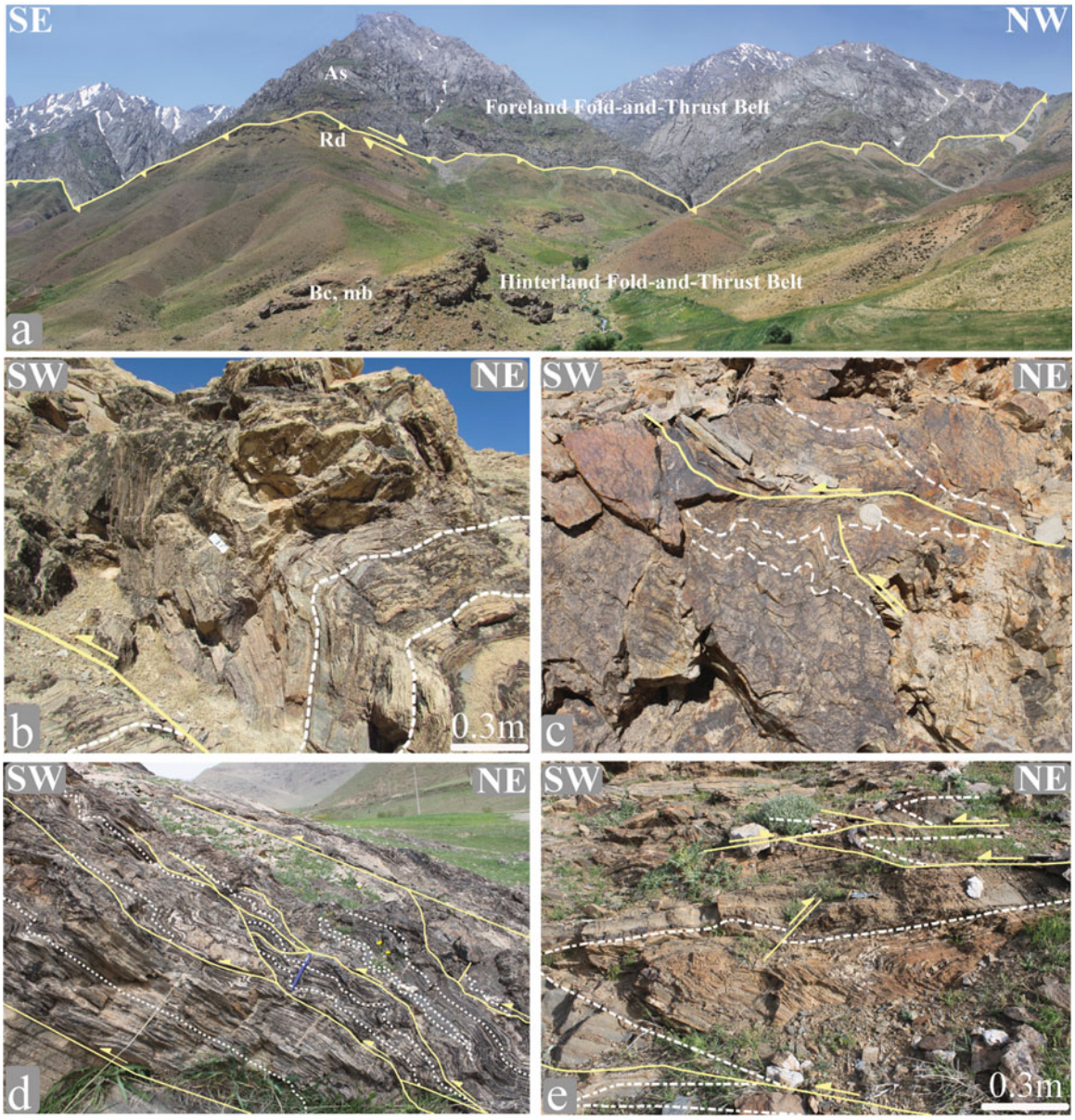

Figure 6. (Colour online) (a) Thrust boundary between hinterland fold-and-thrust belt and foreland fold-and-thrust belt. Basal conglomerate and radiolaritic ocean sediments are thrust over the limestone of the Asmari Formation. (b) Fault-bend folding in the marble layers illustrates the kinematic model of Narr & Suppe (1994). (c) Folded and imbricated quartzo-feldspathic mylonite located in the NW of Azna. (d) Mesoscopic-scale imbricated wedges. (e) Fault-related folds formed by sequential imbrication in the antiformal stack structure in the Permian calc-schist.

Table 1. Details of quartz c-axis fabrics, strain and kinematic vorticity number measurements for samples from the study area.

Sample	Quartz c-axis fabric asymmetry parameters						Finite strain	Vorticity
	C_1	C_2	ω_1	ω_2	ψ	β	R_{xz}	W_k
FM-1	50	5	75	25	81	9	2.7	0.53
FM-2	30	26	31	78	79	11	2.6	0.61
FM-3	42	4	68	27	81	9	2.8	0.54
FM-4	61	8	83	14	81	9	3	0.56
FM-5	51	3	79	21	82	8	2.95	0.5
FM-6	46	7	72	26	82	8	2.7	0.47
FM-7	46	7	68	35	81	9	2.7	0.59
FM-8	50	5	67	32	80	10	2.8	0.59
FM-9	56	2	80	22	82	8	2.5	0.46
FM-10	58	8	81	18	77	13	2.4	0.67

https://doi.org/10.1017/S0016756816000558 Published online by Cambridge University Press

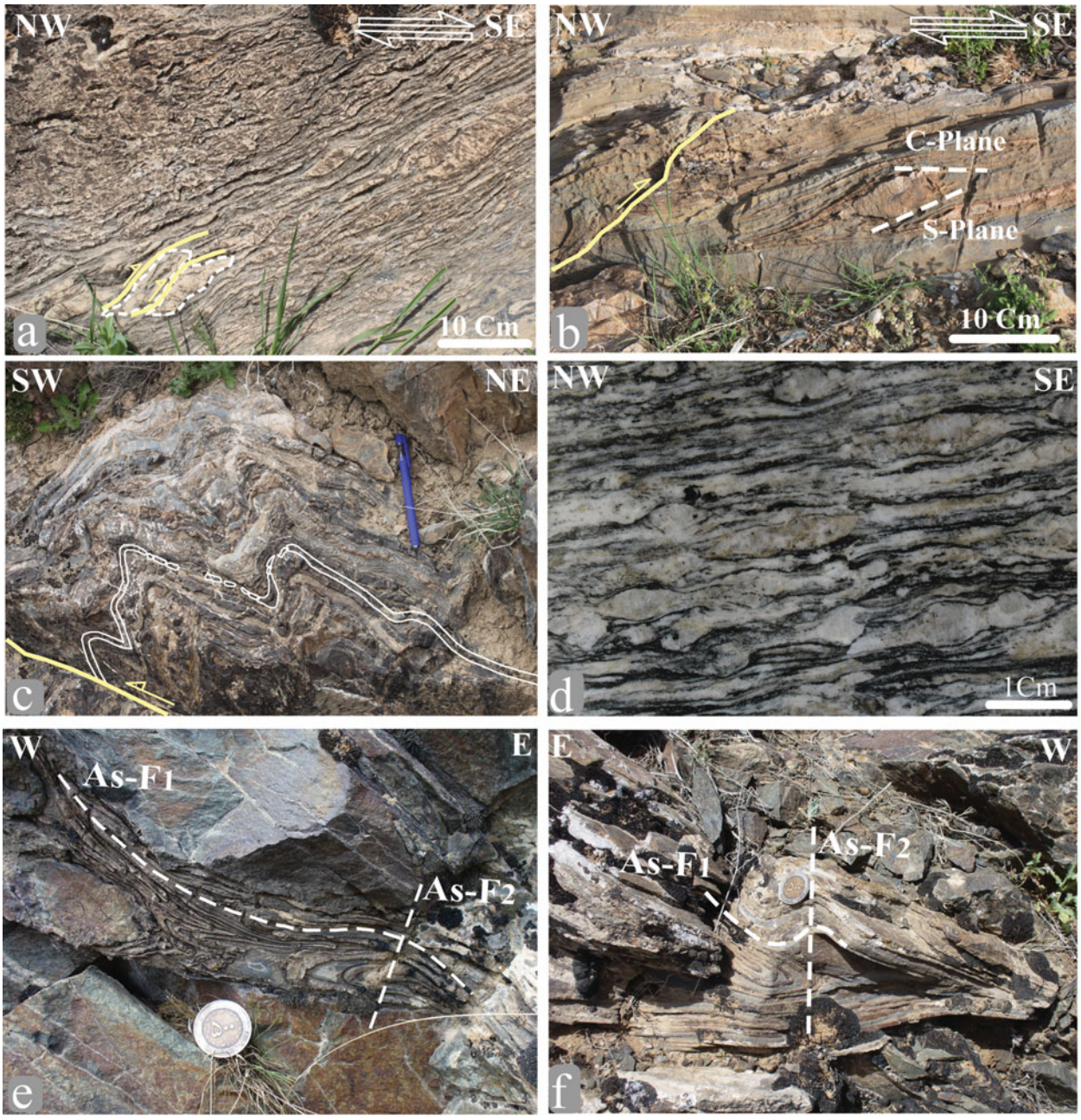

Figure 7. (Colour online) Mesoscopic-scale kinematic indicators of the hinterland fold-and-thrust belt. (a) Sheared boudins, showing piggyback structure. (b) Sigmoidal lenses with monoclinic symmetry which show top-to-the-SE sense of shear. C/S planes are shown. (c) Boudined folded boudins indicate high strain affected by thrusting. (d) Photograph of a polished quartzo-feldspathic mylonite (XZ-plane). (e) Example of type-3 superposed fold pattern. F_1 recumbent fold superposed by F_2 fold. (f) Type-2 superposed fold pattern seen on vertical face (As-F shows the trace of axial surface).

plotted versus the angle φ between major axes and the trace of the foliation in oriented thin sections of feldspar porphyroclasts.

The abundance of deformed feldspar porphyroclasts in mylonite within the quartzo-feldspathic mylonite provided us with a means of estimating the finite strain, using the methods described by Lisle (1985). Feldspar, to which this method is commonly applied, tends to have clasts with a preferred orientation, which will influence their shape in the deformed state and create a challenge in strain analyses. We assume that at the scale of analysis, clasts act as deformed homogeneous objects and passive ellipsoids. Also we assume there was no interaction between clasts during deformation and the rock did not contain a pre-existing fabric. At least 80 feldspar grains were measured on every polished hand specimen surface (XZ-plane). Two-dimensional R_f/φ finite strain data from all the locations have been derived from three-dimensional strain analysis to determine the shape of strain ellipsoids and finite strain analyze. In this method, the finite strains were estimated for ten samples FM-1 to FM-10. The location and R_s value of each sample are shown in Figures 2, 10 and Table.

https://doi.org/10.1017/S0016756816000558 Published online by Cambridge University Press

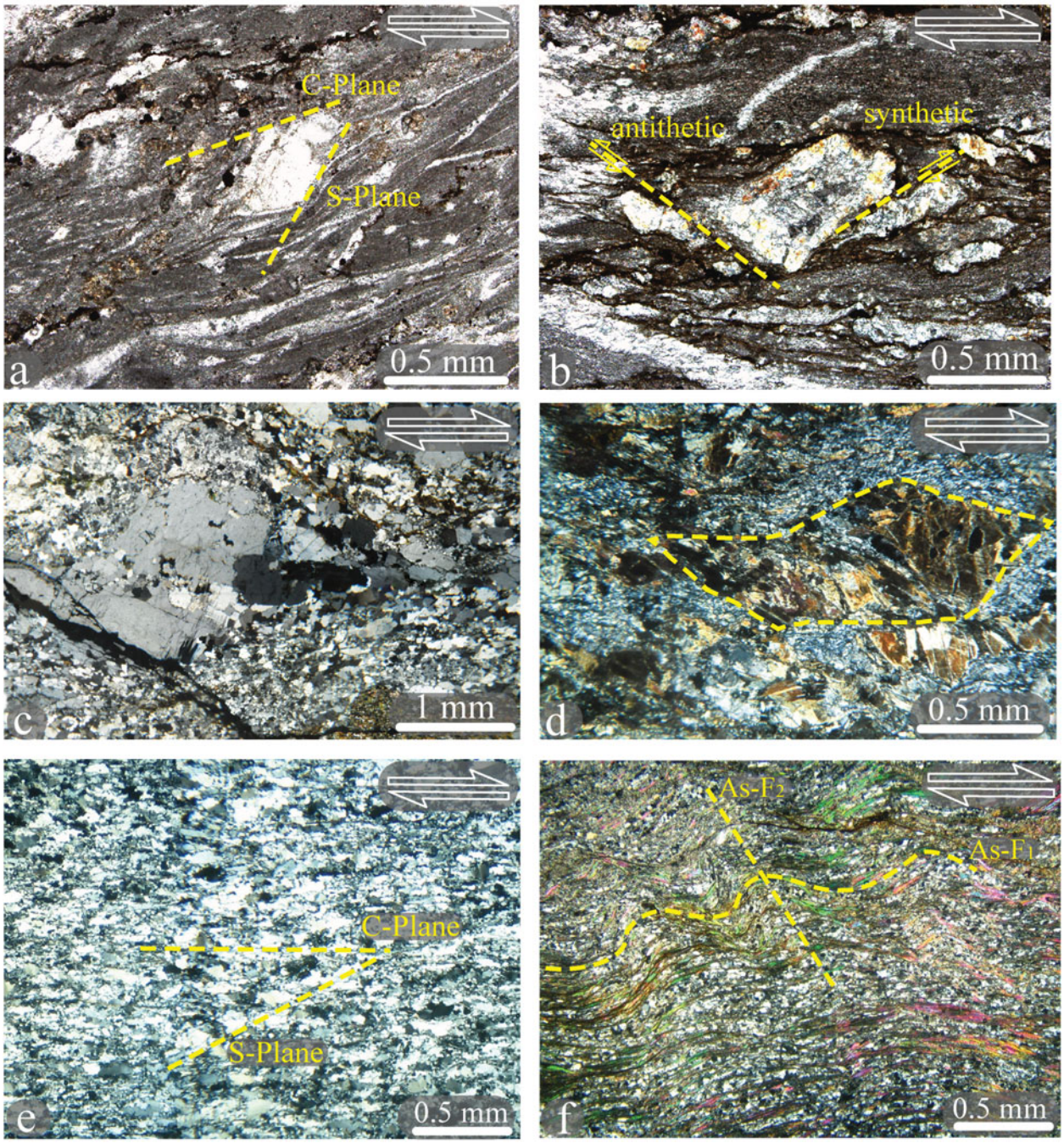

Figure 8. (Colour online) Photo-micrographs showing asymmetrical microstructures. All sections cut perpendicular to the foliation and parallel to the stretching lineation. (a) S/C shear band in mylonitic marble. The movement along the shear band is synthetic with the sense of shear in the surrounding mylonite. (b) Bookshelf structure in mylonitic marble, showing domino-type fragments that consist of synthetic and antithetic micro-faulting. (c) High-grade mylonite derived from quartzo-feldspathic mylonite. K-feldspar porphyroclast is surrounded by fine-grained recrystallized K-feldspar and quartz. (d) High-grade mylonite derived from amphibolite. Hornblende porphyroclast surrounded by a matrix of fine-grained feldspar and quartz. (e) High-grade quartzo-feldspathic mylonite showing C-plane shear band cleavage. (f) Crenulation cleavage, developing along schist with asymmetric micro-folds. S_2 is sub-horizontal and overprints S_1.

10. Finite strain analysis using enhanced normalized Fry method

Quantifying finite strain resulted in calculated fabric ellipsoids from both the R_f/φ and enhanced normalized Fry methods. The enhanced normalized Fry method (Erslev & Ge, 1990) is a graphical technique for determining two-dimensional geological strain by measuring centre-to-centre distance of objects using a certain cut-off radius to remove particles beyond a defined distance from the void centre. The enhanced normalized Fry method was applied to three samples in order to compare the results with those obtained by the R_f/φ method. In the enhanced normalized Fry analysis, centre-to-centre measurements are used and the central points of more than 150 feldspar grains

https://doi.org/10.1017/S0016756816000558 Published online by Cambridge University Press

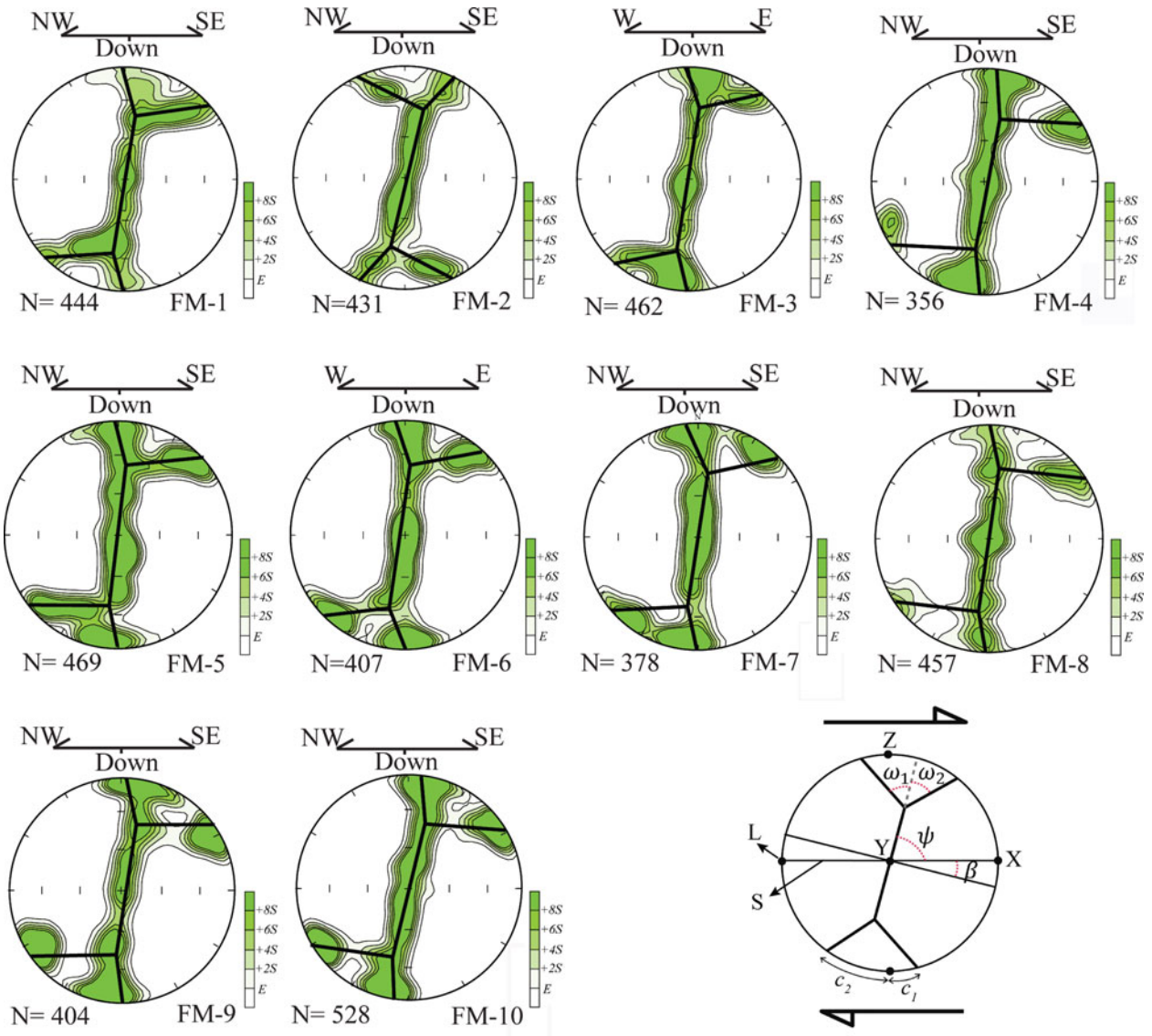

Figure 9. (Colour online) Equal-area, lower-hemisphere stereographic projections of the quartz c-axis fabrics (samples FM-1 to FM-10). The location of the samples is shown in Figures 2 and 3. Fabric skeletons for individual samples from the study area are illustrated (black inset). In all these projections, the foliation (S) is vertical, and stretching lineation (L) within the foliation is horizontal. N = number of grains measured in each sample. C_1 and C_2 show external fabric asymmetry and ω_1 and ω_2 show internal fabric asymmetry (Law, 1990).

per section were used to estimate finite strain. Two-dimensional strain measurements were made on XZ (parallel to stretching lineation and perpendicular to foliation). The finite strain values from the enhanced normalized Fry method for the XZ-plane of samples FM-2, FM-3 and FM-4 are $R_s = 2.6$, 2.58 and 2.87, respectively, confirming the analyses of the R_f/φ method (Fig. 11).

11. Calculating the kinematic vorticity number

The kinematic vorticity number (W_k) is a dimensionless number representing the relative rates of internal rotation and stretching at a point in space and a moment in time (Fossen, 2010, p. 438). W_k has a value that depends on the relative amount of pure shear ($W_k = 0$) versus simple shear ($W_k = 1$); intermediate types are referred to as general shear (Passchier & Trouw, 2005). With respect to the theoretical relationship between vorticity, the orientation of lines with zero instantaneous rotation (the flow apophyses) and instantaneous stretching axes (ISA) (Passchier & Urai, 1988), Wallis (1995) proposed that W_k can be estimated if the strain ratio in the XZ-plane of the finite strain (R_{XZ}) and the angle (β) between the foliation and the orthogonal to the c-axis fabric skeleton (Lister & Williams, 1979) are known. The kinematic vorticity number using the R_{XZ}/β method is sensitive to small changes in the estimated angle β (Grasemann, Fritz & Vannay, 1999; Bailey *et al.* 2004; Law, Searle & Simpson, 2004), and the method becomes unreliable in high-strain zones with $R_{XZ} >$ 10–15 and $\beta < 5$ (Grasemann, Fritz & Vannay, 1999). The vorticity analysis assumes that the vorticity vector is perpendicular to the maximum and minimum

https://doi.org/10.1017/S0016756816000558 Published online by Cambridge University Press

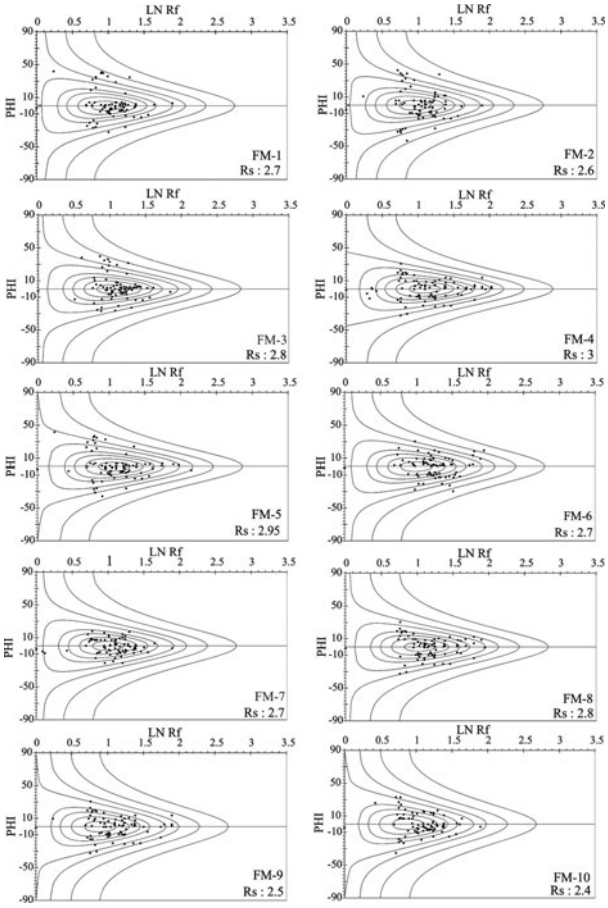

Figure 10. R_f/φ finite strain analyses of feldspar porphyroclasts showing R_i and R_s onion curves for XZ-plane cut perpendicular to the foliation plane.

principal finite strain axes (Law, 2010). Also, flow assumes homogeneous, monoclinic and steady state. However, in a natural system the vorticity of flow may be integrated over space and time (W_k). In the steady-state flow, instantaneous strain (Fossen & Tikoff, 1998; Jiang & Williams, 1998) is considered equal to finite strain (W_m) (Law, Searle & Simpson, 2004). The approximately plane strain suggested by the cross-girdle pattern of the quartz c-axes (Law, 1990) can be satisfied using two-dimensional vorticity analysis (Tikoff & Fossen, 1995).

W_k was calculated using the Wallis (1992, 1995) method in the following formula:

$$W_k = \sin\left\{\tan^1\left[\frac{\sin(2\beta)}{[(R_{xz}+1)/(R_{xz}-1) - \cos(2\beta)] - \cos(2\beta)}\right]\right\} \times \frac{(R_{xz}+1)}{(R_{xz}-1)}$$

Based on our data from ten samples (FM-1 to FM-10; Table 1), application of this method revealed that W_k ranges between 0.46 and 0.67 (Table 1) and the estimated kinematic vorticity number mean is 0.55 ± 0.06.

12. Structural cross-sections

Numerous cross-sections across the Zagros orogenic belt have been published by various workers (e.g. Stöcklin, 1968; Alavi, 1994, 2007; Mohajjel *et al.* 2000; Blanc, Allen & Inger, 2003; McQuarrie, 2004; Sherkati & Letouzey, 2004; Molinaro *et al.* 2005; Agard *et al.* 2005, 2006, 2011; Sarkarinejad & Azizi, 2008; Sarkarinejad & Ghanbarian, 2014). However, these works do not present any detailed structural cross-sections in the hinterland in western Iran. In this research, AA′, BB′ and CC′ cross-sections across the study area have been constructed in order to understand the subsurface structural styles along traverses perpendicular to fold axes and major thrusts (Fig. 2). The cross-sections are constrained according to detailed field observations and high-resolution remote sensing data with modern orthorectification methods.

Constructed cross-sections from SW to NE include two parts of the Zagros orogenic belt: (1) Whole sequences of the Cambrian to Pliocene sedimentary rocks (McQuarrie, 2004) of the foreland fold-and-thrust belt folded on the Hormoz salt detachment surface. Seismic studies confirm the presence of the inverted half-grabens in the upper crust of the foreland basement

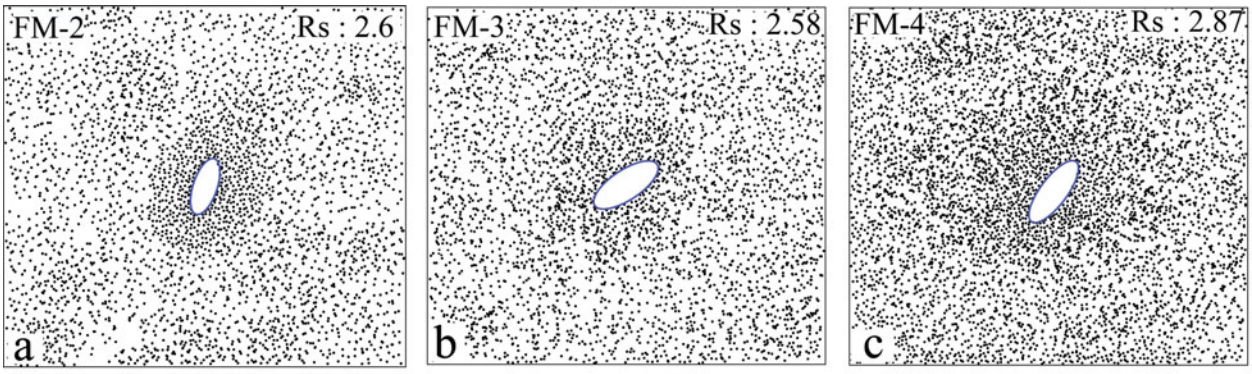

Figure 11. (Colour online) XZ-plane of the finite strain using the enhanced normalized Fry method. The finite strain ellipses show elliptical rims surrounding central vacancies, yielding a high-resolution ellipse, which commonly results from uniform and homogeneous deformation. (a) Sample FM-2, $R_s = 2.6$, (b) sample FM-3, $R_s = 2.58$ and (c) sample FM-4, $R_s = 2.87$.

https://doi.org/10.1017/S0016756816000558 Published online by Cambridge University Press

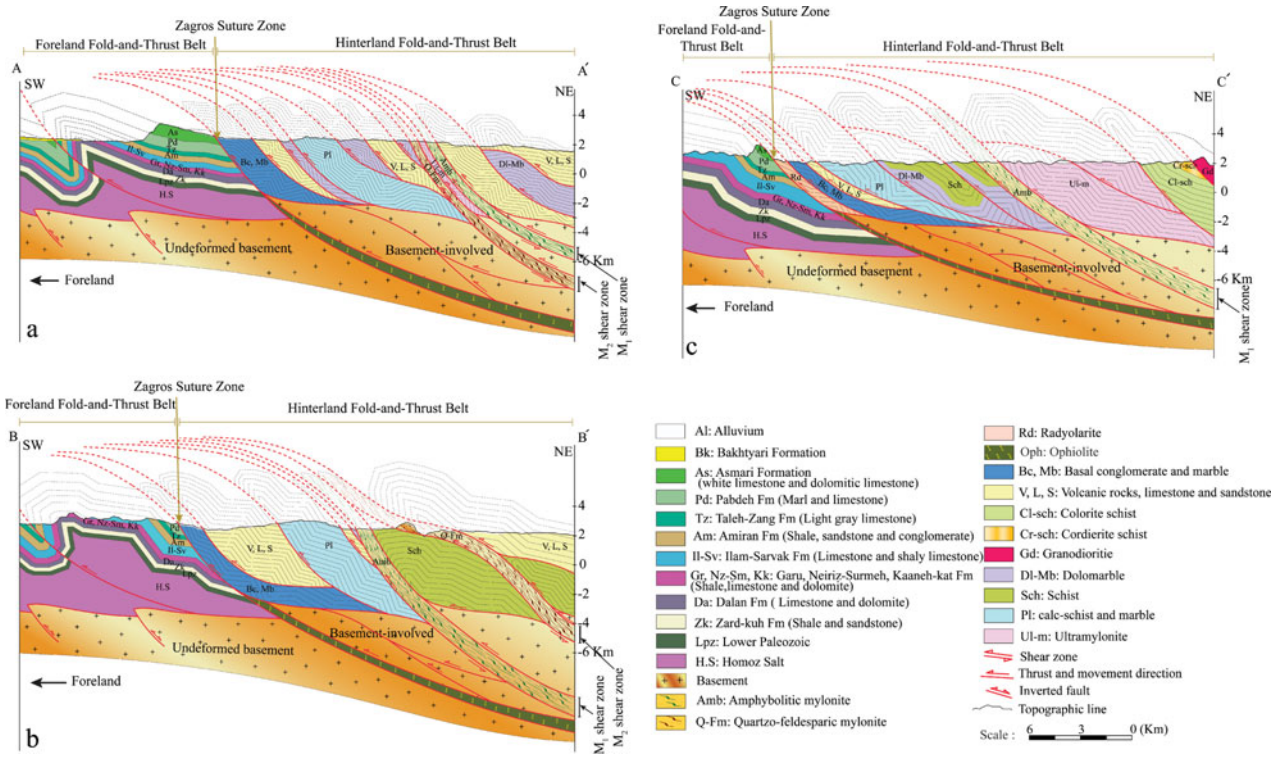

Figure 12. (Colour online) Generalized structural cross-sections across the study area, showing large-scale imbricated thrusts, basement-involved mylonite nappes and Palaeozoic and Mesozoic sedimentary cover sequences. Black lines across the geological map (Fig. 2) show the position of the AA', BB' and CC' cross-sections. The strike of cross-sections is NE–SW. (a), (b) and (c) present AA', BB' and CC' cross-sections, respectively.

(Sepehr & Cosgrove, 2004). (2) The hinterland fold-and-thrust belt is dominated by in-sequence thrusting, duplex structures and exhumation of the quartzo-feldspathic and amphibolitic mylonite nappes (M_1 and M_2 shear zones). Thrusts are related to folds (Suppe, 1983) which were constructed using the kink method (Faill, 1969, 1973). Several map-scale fault-bend folds crop out in the study area and are shown in the cross-sections (Fig. 12). Imbricate stacks are created fault-bend folding with NW-striking and NE-dipping.

The suture zone is considered as the boundary between foreland and hinterland fold-and-thrust Belts which are recognized by outcrops of ophiolites and radiolarian cherts in this zone. Ophiolites are not exposed in this part of the Zagros suture zone. As mentioned before, ophiolites are slices of Neo-Tethyan oceanic crust that obducted during the Turonian–Cenomanian within the Zagros accretionary prism (Sarkarinejad, Godin & Faghih, 2009).

13. Discussion

The Zagros orogenic belt resulted from the NE subduction of Neo-Tethys oceanic crust below the Iranian microcontinent and subsequent convergence of the Arabian and Eurasian plates from the late Cretaceous to the Present (Stöcklin, 1968; Ricou, 1971; Takin, 1972; Dewey *et al.* 1973; Berberian & King, 1981; Koop & Stoneley, 1982; Alavi, 1994; Blanc, Allen & Inger, 2003; McClay *et al.* 2004; McQuarrie, 2004; Sarkarinejad & Azizi, 2008).

The Zagros Thrust System is an array of oblique-slip thrust sheets, shear zones, imbricate fans and duplex structures with involved components of both dip-slip and strike-slip that are related to each other geometrically, kinematically and mechanically and are associated with the Zagros dextral inclined transpression zone. This thrust system developed at the boundaries of the dextral inclined transpression zone (Sarkarinejad & Azizi, 2008). Exhumation of the mylonites and ductile materials is bounded to these boundaries. Mylonitic nappes have been exhumed along the Zagros hinterland basement-involved located in the Zagros Thrust System, corroborating thick-skinned tectonics. The Tutak gneiss dome exposes a basement window exhumed in the hinterland of the Zagros orogenic belt (Sarkarinejad & Alizadeh, 2009). The hinterland fold-and-thrust belt developed in the internal portion of the orogenic belt, and thrusting involved deeper crustal rocks and basement (Vaníček & Vaníček, 2008, p. 195).

Several kinematic models have been developed to explain diverse fault-related fold mechanisms in orogens. These include a detachment fold created by layers riding parallel to a thrust and without upward propagation of the thrust. In fault propagation folds, the fold forms beyond the tip of a blind thrust where propagation along the detachment surface has ceased but displacement on the thrust continues. Fault-bend folds are developed by movements over thrust ramps (Suppe, 1983)

https://doi.org/10.1017/S0016756816000558 Published online by Cambridge University Press

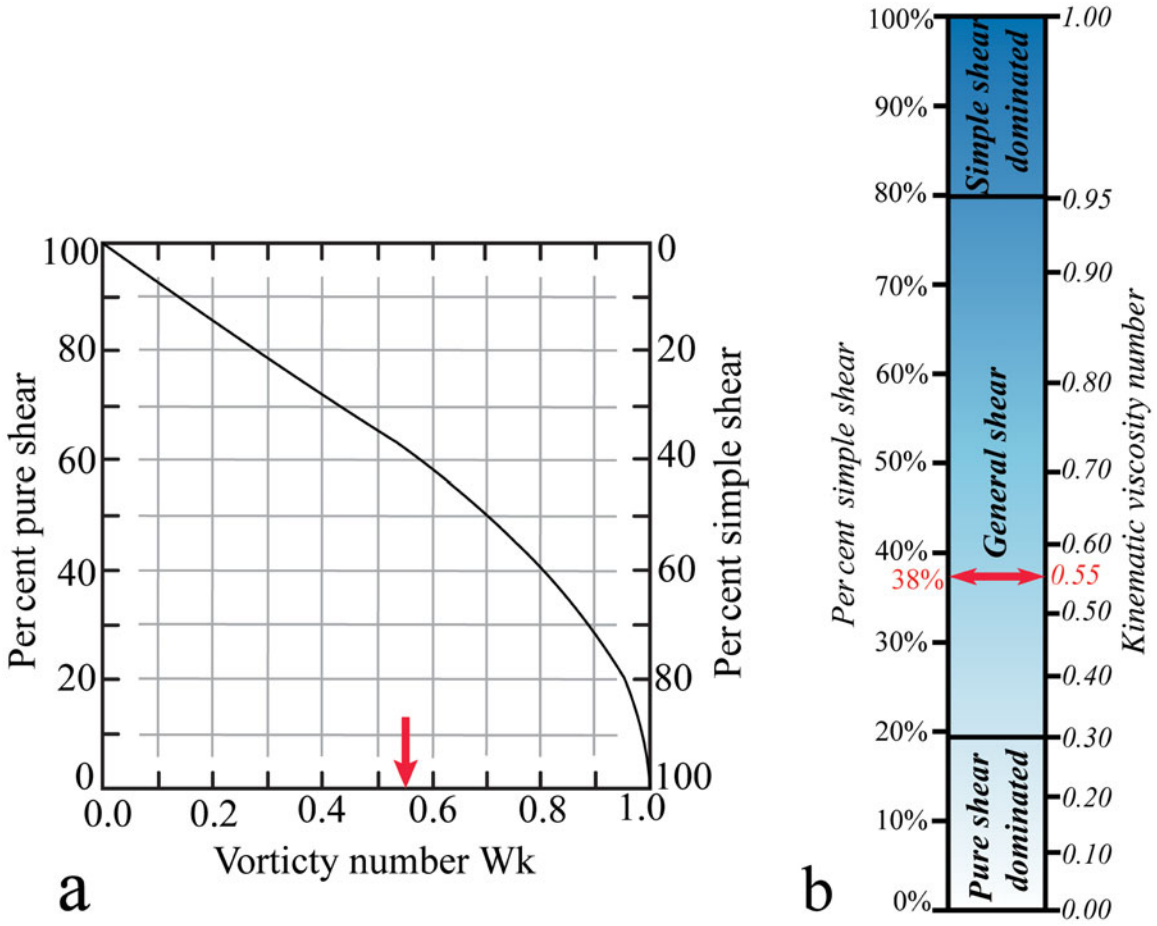

Figure 13. (Colour online) (a) Relation between kinematic vorticity number (W_k) and components of pure and simple shear for instantaneous two-dimensional flow (modified after Law, Searle & Simpson, 2004). The mean estimated $W_k = 0.55$ (arrow) for mylonite samples indicates 62 % pure shear and 38 % simple shear components. (b) Relation between the W_k value and per cent simple shear (modified after Forte & Bailey, 2007).

and show top-to-the-foreland motion. The interpreted structures in the study area shown in the three cross-sections (Fig. 12) reflect a combination of field data and kink-band fault-bend fold models of Suppe (1983), map-scale oblique-slip thrusts, duplex structures and basement-involved mylonite nappes. Ongoing shortening causes older thrusts to override younger ones, producing imbricate thrust systems and antiformal stacks

In thick-skinned tectonics, thrust wedges and steep faults penetrate the basement, giving rise to basement blocks bounded by faults, with subsequent uplift and partial exhumation of basement rocks at the crustal scale (Escher & Beaumont, 1997; Poblet & Lisle, 2011).

Highly strained ductile rocks in natural shear zones can be exhumed from deep crustal levels during transpressional deformation (Sanderson & Marchini, 1984; Jones *et al.* 2004). Most orogenic belts have non-planar zone boundaries and wedge-shaped overall geometries (Jones *et al.* 2004). Inclined convergence and shortening were accommodated by imbricate thrust systems and duplex structures generated in the fold-and-thrust belts along the foreland and hinterland of the Zagros orogenic belt. Transpression was heterogeneously distributed within the shear zone system.

Basement-involved mylonitic nappes are exposed along flexural-slip imbricate thrust stacks and are enucleated within the basement by M_1 and M_2 shear zones (Fig. 12). Exhumed quartzo-feldspathic and amphibolitic mylonites indicate medium to high-grade metamorphic conditions of deformation. Fault-bend folds and M_1 and M_2 shear zones are formed by ongoing dextral inclined transpressional regime during D_3 deformation.

Kinematic vorticity analysis demonstrates that regional ductile deformation involved general shearing with a combination of simple and pure shear (Fig. 13b). Given the assumptions involved in the method used, the mean kinematic vorticity (W_m) calculated from ten specimens indicates a pure shear component of 62 % and a simple shear component of 38 % for the Zagros mylonites (Fig. 13a) that are close to the basal thrust of the hinterland fold-and-thrust belt. Based on this ratio, the estimated θ angle between the maximum instantaneous strain axis (ISA_1) and the transpressional zone boundary is 17°. The angle of flow apophyses (α)

https://doi.org/10.1017/S0016756816000558 Published online by Cambridge University Press

indicates a convergence angle between the Iranian and Afro-Arabian plates of 57° along the exhumation of M_2 mylonitic nappe.

During plastic deformation and dynamic recrystallization, the opening angle of quartz c-axis girdles relates directly to the temperature of deformation (Tullis, Christie & Griggs, 1973; Lister & Hobbs, 1980; Lister & Dornsiepen, 1982). The geothermometer (Kruhl, 1996) modified by Law, Searle & Simpson (2004) and Morgan & Law (2004), implies that these rocks deformed at temperatures ranging between 425 ± 50 °C and 540 ± 50 °C. Quartz grains are generally recrystallized and form elongate polycrystalline ribbons. Quartzo-feldspathic mylonites show a strong foliation and lineation defined by the alignments of mica. Monoclinic cross-girdle quartz c-axis fabrics and the orthogonal relationship between fabric skeleton and foliation (ten samples in Fig. 9) are consistent with approximately plane strain conditions (Frassi *et al.* 2009).

14. Conclusions

The purpose of this research is to investigate collisional and convergent processes in a transpressional setting that resulted from oblique convergence between the Iranian microcontinent and the Afro-Arabian plates after the intervening portion of Neo-Tethys closed. Strain partitioning across the mylonitic nappes involved simultaneous dip-slip and strike-slip displacements in the ductile thrust system that developed during inclined dextral transpression.

Three phases of deformation formed the various structures. Quartz c-axis fabrics show asymmetrical type-1 cross girdles, indicating non-coaxial plane strain deformation. The mean value of the kinematic vorticity (W_m) was 0.55 ± 0.06, indicating a general shear deformation with 62 % pure and 38 % simple shear components in the Doroud–Azna area. Mesoscopic and microscopic shear sense indicators confirm dextral transpression (top-to-the-SE). The angle between the maximum horizontal instantaneous strain axis and the plate boundary ($\alpha = 57°$) shows that the plate convergence causing the Zagros Thrust System was oblique. Based on opening angles of quartz girdles, deformation temperatures varied from 425 ± 50 °C to 540 ± 50 °C, which indicates amphibolite facies conditions. All of the structural evidence indicates that the hinterland fold-and-thrust belt of the Zagros orogen was characterized by thick-skinned deformation; basement was strongly involved and exhumed as mylonite nappes.

Acknowledgements. The authors wish to thank Professor C. J. Talbot and Dr David Iacopini for constructive reviews and valuable editorial comments. We also thank Professor Mark B. Allen, Editor-in-Chief of the *Geological Magazine*, for accepting the manuscript, and Professor Jan Tullis who critically reviewed and improved the manuscript. This research was supported by a Shiraz University Research Council (SURC) grant which is gratefully acknowledged.

References

AGARD, P., MONIE, P., GERBER, W., OMRANI, J., MOLINARO, M., MEYER, B., LABROUSSE, L., VRIELYNCK, B., JOLIVET, L. & YAMATO, P. 2006. Transient, synobduction exhumation of Zagros blueschists inferred from P-T, deformation, time, and kinematic constraints: implications for Neotethyan wedge dynamics. *Journal of Geophysical Research* **111**, 1978–2012.

AGARD, P., OMRANI, J., JOLIVET, L. & MOUTHEREAU, F. 2005. Convergence history across Zagros (Iran): constraints from collisional and earlier deformation. *International Journal of Earth Sciences* **94**, 401–19.

AGARD, P., OMRANI, J., JOLIVET, L., WHITECHURCH, H., VRIELYNCK, B., SPAKMAN, W., MONIE, P., MEYER, B. & WORTEL, R. 2011. Zagros orogeny: a subduction-dominated process. *Geological Magazine* **148**, 692–725.

ALAVI, M. 1994. Tectonics of the Zagros orogenic belt of Iran: new data and interpretations. *Tectonophysics* **229**, 211–38.

ALAVI, M. 2007. Structures of the Zagros fold-thrust belt in Iran. *American Journal of Science* **307**, 1064–95.

ALLEN, M. B., JACKSON, J. & WALKER, R. 2004. Late Cenozoic reorganization of the Arabia-Eurasia collision and comparison of the short-term and long-term deformation rates. *Tectonics* **23**(2). doi: 10.1029/2004TC001695.

AUTHEMAYOU, C., BELLIER, O., CHARDON, D., MALEKZADE, Z. & ABBASSI, M. 2005. Role of Kazerun fault system in active deformation of the Zagros fold-and-thrust belt (Iran). *Comptes Rendus de l'Académie des Sciences* **337**, 539–45.

BAILEY, C. M. & EYSTER, E. L. 2003. General shear deformation in the Pinaleno Mountains metamorphic core complex, Arizona. *Journal of Structural Geology* **25**, 1883–93.

BERBERIAN, M. & KING, G. C. P. 1981. Towards a paleogeography and tectonic evolution of Iran. *Canadian Journal of Earth Sciences* **12**, 210–65.

BERTHE, D., CHOUKROUNE, P. & GAPAIS, D. 1979. Orientations préférentielles du quartz et orthogneissification progressive en régime cisaillant: l'exemple du cisaillement sud-armoricain. *Bulletin Minéral* **102**, 265–72.

BERTHE, D., CHOUKROUNE, P. & JEGOUZO, P. 1979. Orthogeneiss, mylonite and non-coaxial deformation of granites: the example of South Armorican shear zone. *Journal of Structural Geology* **1**, 31–42.

BLANCE, E. J., ALLEN, M. & INGER, S. 2003. Structural styles in the Zagros Simple Folded Zone, Iran. *Journal of the Geological Society* **160**, 401–12.

DEWEY, J. F., PITMAN, W. C., RYAN, W. B. F. & BONNIN, J. 1973. Plate tectonics and the evolution of the Alpine system. *Geological Society of America Bulletin* **84**, 3137–80.

DUNNET, D. 1969. A technique of finite strain analysis using elliptical particles. *Tectonophysics* **7**, 117–36.

ELLIOTT, D. 1983. The construction of balanced cross-sections. *Journal of Structural Geology* **5**, 101.

ERSLEV, E. A. & GE, H. 1990. Least squares center-to-center and mean object ellipse fabric analysis. *Journal of Structural Geology* **8**, 1047–59.

ESCHER, A. & BEAUMONT, C. 1997. Formation, burial and exhumation of basement nappes at crustal scale: a

https://doi.org/10.1017/S0016756816000558 Published online by Cambridge University Press

geometric model based on the Western Swiss-Italian Alps. *Journal of Structural Geology* **19**, 955–74.

ETCHECOPAR, A. 1977. A plane model of progressive deformation in polycrystalline aggregates. *Tectonophysics* **39**, 121–39.

ETCHECOPAR, A. & VASSEUR, G. 1987. A 3D kinematic model of fabric development in polycrystalline aggregates: comparison with experimental and natural examples. *Journal of Structural Geology* **9**, 705–17.

FAILL, R. T. 1969. Kink band structures in the Valley and Ridge Province, central Pennsylvania. *Geological Society of America Bulletin* **80**, 2539–50.

FAILL, R. T. 1973. Kink band folding, Valley and Ridge Province, Pennsylvania. *Geological Society of America Bulletin* **84**, 1289–314.

FORTE, A. M. & BAILEY, C. M. 2007. Testing the utility of the porphyroclast hyperbolic distribution method of kinematic vorticity analysis. *Journal of Structural Geology* **29**, 983–1001.

FOSSEN, H. 2010. *Structural Geology*. Cambridge: Cambridge University Press, 457 pp.

FOSSEN, H. & TIKOFF, B. 1993. The deformation matrix for simultaneous simple shearing, pure shearing and volume change, and its application to transpression-transtension tectonics. *Journal of Structural Geology* **15**, 413–22.

FOSSEN, H., TIKOFF, B. & TEYSSIER, C. 1994. Strain modeling of transpression and transtension deformation. *Norsk Geologisk Tidsskrift* **74**, 134–45.

FRASSI, C., CAROSI, R., MONTOMOLI, C. & LAW, R. D. 2009. Kinematics and vorticity of flow associated with post-collisional oblique transpression in the Variscan Axial Zone of northern Sardinia (Italy). *Journal of Structural Geology* **31**, 1458–71.

GOMEZ-RIVAS, E., BONSE, P. D., GRIERA, A., CARRERAS, J., DRUGUET, E. & EVANS, L. 2007. Strain vorticity analysis using small-scale faults associated drag folds. *Journal of Structural Geology* **29**, 1882–99.

GOODARZI, M. 2010. *Geological Map of the Doroud Area*. Scale 1:100000. Tehran: National Iranian Oil Company.

GOSCOMBE, B., PASSCIER, C. W. & HAND, M. 2004. Boudinage classification: end-member boudin types and modified boudin structures. *Journal of Structural Geology* **26**, 739–63.

GRASEMANN, B., FRITZ, H. & VANNAY, J. C. 1999. Quantitative kinematic flow analysis from the Main Central Thrust Zone (NW-Himalaya, India): implications for a decelerating strain path and the extrusion of orogenic wedges. *Journal of Structural Geology* **21**, 837–53.

HOLCOMBE, R. J. & LITTLE, T. A. 2001. A sensitive vorticity gauge using rotated prophyroblasts and its application to rocks adjacent to the Alpine fault, New Zealand. *Journal of Structural Geology* **23**, 979–89.

IACOPINI, D., CAROSI, R., MONTOMOLI, C. & PASSCHIER, C. W. 2008. Strain analysis and vorticity of flow in the Northern Sardinian Variscan Belt: recognition of a partitioned oblique deformation event. *Tectonophysics* **446**, 77–96.

JESSEL, M. W. & LISTER, G. S. 1990. A simulation of the temperature dependence of quartz fabrics. In *Deformation Mechanisms, Rheology and Tectonics* (eds R. J. Knipe & E. H. Potter), pp. 353–62. Geological Society of London, Special Publication no. 54.

JESSUP, M. J., LAW, R. D. & FRASSI, C. 2007. The rigid grain net (RGN): an alternative method for estimating mean kinematic vorticity number (W_m). *Journal of Structural Geology* **29**, 411–21.

JONES, R. R., HOLDSWORTH, R. E., CLEGG, P., MCCAFFREY, K. & TAVARNELLI, E. 2004. Inclined transpression. *Journal of Structural Geology* **26**, 1531–48.

JONES, R. & TANNER, G. P. W. 1995. Strain partitioning in transpression zones. *Journal of Structural Geology* **17**, 793–802.

KOOP, W. J. & STONELEY, R. 1982. Subsidence history of the Middle East Zagros Basin, Permian to recent. *Philosophical Transactions of the Royal Society of London* **305**, 149–68.

KRUHL, J. H. 1996. Prism- and basal-plane parallel subgrain boundaries in quartz: a microstructural geothermobarometer. *Journal of Metamorphic Geology* **14**, 581–9.

LAW, R. D. 1987. Heterogeneous deformation and quartz crystallographic fabric transitions: natural examples from the Moine thrust zone at the Stack of Glencoul, northern Assynt. *Journal of Structural Geology* **9**, 819–34.

LAW, R. D. 1990. Crystallographic fabrics: a selective review of their applications to research in structural geology. In *Deformation Mechanisms, Rheology and Tectonics* (eds R. J. Knipe & E. H. Potter), pp. 335–52. Geological Society of London, Special Publication no. 54.

LAW, R. D. 2010. Moine Thrust zone mylonites at the Stack of Glencoul: II – results of vorticity analyses and their tectonic significance. In *Continental Tectonics and Mountain Building: The Legacy of Peach and Horne* (eds R. D. Law, R. W. H. Butler, R. E. Holdsworth, M. Krabbendam & R. A. Strachan), pp. 579–602. Geological Society of London, Special Publication no. 335.

LAW, R. D., KNIPE, R. J. & DAYAN, H. 1984. Strain path partitioning within thrust sheets: microstructural and petrofabric evidence from the Moine Thrust zone at Loch Eriboll, northwest Scotland. *Journal of Structural Geology* **6**, 477–97.

LAW, R. D., SEARLE, M. P. & SIMPSON, R. L. O. 2004. Strain, deformation temperatures and vorticity of flow at the top of the Greater Himalayan slab, Everest Massif, Tibet. In *Channel Flow, Ductile Extrusion and Exhumation in Continental Collision Zones* (eds R. D. Law, M. P. Searle & L. Godlin), pp. 305–20. Geological Society of London, Special Publication no. 161.

LISLE, R. J. 1985. *Geological Strain Analysis: A Manual for the Rf/ϕ Method*. New York: Pergamon Press, 99 pp.

LISTER, G. S. 1977. Crossed girdle c-axis fabrics in quartzites plastically deformed by plane strain and progressive simple shear. *Tectonophysics* **39**, 51–4.

LISTER, G. S. & DORNSIEPEN, U. F. 1982. Fabric transitions in the Saxony granulite terrain. *Journal of Structural Geology* **4**, 81–92.

LISTER, G. S. & HOBBS, B. E. 1980. The simulation of fabric development during plastic deformation and its application to quartzite: the influence of deformation history. *Journal of Structural Geology* **2**, 355–70.

LISTER, G. S. & PATERSON, M. S. 1979. The simulation of fabric development during plastic deformation and its application to quartzite: fabric transitions. *Journal of Structural Geology* **1**, 99–115.

LISTER, G. S., PATERSON, M. S. & HOBBS, B. E. 1978. The simulation of fabric development in plastic deformation and its application to quartzite: the model. *Tectonophysics* **45**, 107–58.

LISTER, G. S. & SNOKE, A. W. 1984. S-C mylonites. *Journal of Structural Geology* **6**, 617–38.

LISTER, G. S. & WILLIAMS, P. F. 1979. Fabric development in shear zones: theoretical controls and observed phenomena. *Journal of Structural Geology* **1**, 283–98.

https://doi.org/10.1017/S0016756816000558 Published online by Cambridge University Press

MARQUES, F. O., SCHMID, D. W. & ANDERSEN, T. B. 2007. Applications of inclusion behavior models to a major shear zone system: the Nordfjord-Sogn Detachment Zone in western Norway. *Journal of Structural Geology* **29**, 1622–31.

MCCLAY, K. R., WHITEHOUSE, P. S., DOOLEY, M. & RICHARDS, M. 2004. 3D evolution of fold and thrust belts formed by oblique convergence. *Marine and Petroleum Geology* **21**, 857–77.

MCQUARRIE, N. 2004. Crustal scale geometry of the Zagros fold-thrust belt, Iran. *Journal of Structural Geology* **26**, 519–35.

MOHAJJEL, M. & FERGUSSON, C. L. 2000. Dextral transpression in Late Cretaceous continental collision, Sanandaj-Sirjan Zone, western Iran. *Journal of Structural Geology* **22**, 1125–39.

MOLINARO, M., LETUEMY, P., GUEZOU, J. C., FRIZON DE LAMOTTE, D. & ESHRAGHI, S. A. 2005. The structure and kinematics of the southeastern Zagros fold-thrust belt, Iran: from thin-skinned to thick-skinned tectonics. *Tectonics* **24**, 1–19.

MORGAN, S. S. & LAW, R. D. 2004. Unusual transition in quartzite dislocation creep regimes and crystal slip systems in the aureole of the Eureka Valley–Joshua Flat–Beer Creek pluton, California: a case for anhydrous conditions created by decarbonation reactions. *Tectonophysics* **384**, 209–31.

NARR, W. & SUPPE, J. 1994. Kinematics of basement-involved compressive structures. *American Journal of Science* **294**, 802–60.

PASSCHIER, C. W. 1987. Stable positions of rigid objects in non-coaxial flow – a study in vorticity analysis. *Journal of Structural Geology* **9**, 679–90.

PASSCHIER, C. W. & SIMPSON, C. 1986. Porphyroclast systems as kinematic indicators. *Journal of Structural Geology* **8**, 831–44.

PASSCHIER, C. W. & TROUW, R. A. J. 2005. *Microtectonics*. Berlin: Springer, 366 pp.

PASSCHIER, C. W. & URAI, J. L. 1988. Vorticity and strain analysis using Mohr diagrams. *Journal of Structural Geology* **10**, 755–63.

PLATT, J. P. & BEHRMANN, J. H. 1986. Structures and fabrics in a crustal scale shear zone, Betic Cordilleras, SE Spain. *Journal of Structural Geology* **8**, 15–34.

POBLET, J. & LISLE, R. J. 2011. Kinematic evolution and structural styles of fold-and-thrust belts. In *Kinematic Evolution and Structural Styles of Fold-And-Thrust Belts* (eds J. Poblet & R. J. Lisle), pp. 1–24. Geological Society of London, Special Publication no. 349.

RAMSAY, J. G. 1962. The geometry and mechanics of formation of 'similar' type folds. *The Journal of Geology* **70**, 309–27.

RAMSAY, J. G. 1967. *Folding and Fracturing of Rocks*. New York: McGraw Hill, 568 pp.

RAMSAY, J. G. & HUBER, M. I. 1983. *The Techniques of Modern Structural Geology, Volume 1: Strain Analysis*. London: Academic Press, 307 pp.

RAMSAY, J. G. & HUBER, M. I. 1987. *The Techniques of Modern Structural Geology. Volume 2: Folds and Fractures*. London: Academic Press, 392 pp.

REGARD, V., BELLIER, O., THOMAS, J. C., ABBASSI, M., MERCIER, J., SHABANIAN, E., FEGHHI, K. & SOLEYMANI, S. 2004. Accommodation of Arabia-Eurasia convergence in the Zagros-Makran transfer zone, SE Iran: a transition between collision and subduction through a young deforming system. *Tectonics* **23**, 1–24.

RICOU, L. E. 1971. Le croissant ophiolitique péri-arabe. Une ceinture de nappes mises en place au Crétacé supérieur. *Revue de Géographie Physique et de Géologie Dynamique* **13**, 327–50.

SAHANDI, M. R., RADFAR, J., HOSEINIDOUST, J., MOHAJJEL, M., CHAICHI, Z. & HADDADAN, M. 2006. *Geological Map of the Shazand Area*. Scale 1:100000. Tehran: Geological Survey of Iran.

SANDERSON, D. J. & MARCHINI, W. R. D. 1984. Transpression. *Journal of Structural Geology* **6**, 449–58.

SARKARINEJAD, K. 1999. Tectonic finite strain analysis: using Ghouri deformed conglomerate, Neyriz area, southwestern Iran. *Iranian Journal of Science and Technology* **23**, 351–63.

SARKARINEJAD, K. 2005. Structures and microstructures related to steady-state mantle flow in the Neyriz ophiolite, Iran. *Journal of Asian Earth Sciences* **25**, 859–81.

SARKARINEJAD, K. 2007. Quantitative finite strain and kinematic flow analyses along the Zagros transpression zone, Iran. *Tectonophysics* **442**, 49–65.

SARKARINEJAD, K. & ALIZADEH, A. 2009. Dynamic model for the exhumation of the Tutak gneiss dome within a bivergent wedge in the Zagros Thrust System of Iran. *Journal of Geodynamics* **47**, 201–9.

SARKARINEJAD, K. & AZIZI, A. 2008. Slip partitioning and inclined dextral transpression along the Zagros Thrust System, Iran. *Journal of Structural Geology* **30**, 116–36.

SARKARINEJAD, K., FAGHIH, A. & GRASEMANN, B. 2008. Transpressional deformations within the Sanandaj-Sirjan Metamorphic Belt (Zagros Mountains, Iran). *Journal of Structural Geology* **30**, 818–26.

SARKARINEJAD, K. & GHANBARIAN, M. A. 2014. The Zagros hinterland fold-and-thrust belt in-sequence thrusting, Iran. *Journal of Asian Earth Sciences* **85**, 66–79.

SARKARINEJAD, K., GODIN, L. & FAGHIH, A. 2009. Kinematic vorticity flow analysis and $^{40}Ar/^{39}Ar$ geochronology related to inclined extrusion of the HP-LT metamorphic rocks along the Zagros accretionary prism, Iran. *Journal of Structural Geology* **31**, 691–706.

SARKARINEJAD, K., PARTABIAN, A., FAGHIH, A. & KUSKY, T. M. 2012. Usage of strain and vorticity analyses to interpret large-scale fold mechanisms along the Sanandaj-Sirjan metamorphic belt, SW Iran. *Geological Journal* **47**, 99–110.

SEPEHR, M. & COSGROVE, J. W. 2004. Structural framework of the Zagros fold–thrust belt, Iran. *Marine and Petroleum Geology* **21**, 829–43.

SHERKATI, S. & LETOUZEY, J. 2004. Variation of structural style and basin evolution in the central Zagros (Izeh zone and Dezful Embayment), Iran. *Marine and Petroleum Geology* **2**, 535–54.

SIMPSON, C. & DE PAOR, D. G. 1993. Strain and kinematic analysis in general shear zones. *Journal of Structural Geology* **15**, 1–20.

SIMPSON, C. & SCHIMID, S. 1983. An evaluation of criteria to deduce the sense of movement in sheared rocks. *Geological Society of America Bulletin* **94**, 1281–8.

STAMPFLI, G. M., MOSAR, J., FAVRE, P., PILLEVUIT, A. & VANNAY, J. C. 2001. Permo-Mesozoic evolution of the western Tethys realm: the Neo-Tethys East Mediterranean basin connection. *Mémoires du Muséum national d'histoire naturelle* **186**, 51–108.

STÖCKLIN, J. 1968. Structural history and tectonics of Iran: a review. *Bulletin of the American Association of Petroleum Geologists* **52**, 1229–58.

SULLIVAN, W. A. 2008. Significance of transport-parallel strain variations in part of the Raft River shear zone,

https://doi.org/10.1017/S0016756816000558 Published online by Cambridge University Press

Raft River Mountains, Utah, USA. *Journal of Structural Geology* **30**, 138–58.

SUPPE, J. 1983. Geometry and kinematics of fault-bend folding. *American Journal of Sciences* **283**, 648–721.

TAKIN, M. 1972. Iranian geology and continental drift in the Middle East. *Nature* **235**, 147–50.

TALEBIAN, M. & JACKSON, J. 2004. A reappraisal of earthquake focal mechanisms and active shortening in the Zagros mountains of Iran. *Geophysical Journal International* **156**, 506–26.

TATAR, M., HATZFELD, D. & GHAFORY-ASHTIYANI, M. 2004. Tectonics of the Central Zagros (Iran) deduced from microearthquake seismicity. *Geophysical Journal International* **156**, 255–66.

TEYSSIER, C., TIKOFF, B. & MARKLEY, M. 1995. Oblique plate motion and continental tectonics. *Geology* **23**, 447–50.

THIGPEN, J. R., LAW, R. D., LLOYD, G. E., BROWN, S. J. & COOK, B. 2010. Deformation temperatures, vorticity of flow and strain symmetry in the Loch Eriboll mylonites, NW Scotland: implications for the kinematic and structural evolution of the northernmost Moine thrust zone. In *Continental Tectonics and Mountain Building: The Legacy of Peach and Horne* (eds R. D. Law, R. W. H. Butler, R. E. Holdsworth, M. Krabbendam & R. A. Strachan), pp. 623–62. Geological Society of London, Special Publication no. 335.

TIKOFF, B. & FOSSEN, H. 1995. The limitations of three-dimensional kinematic vorticity analysis. *Journal of Structural Geology* **17**, 1771–84.

TIKOFF, B. & TEYSSIER, C. 1994. Strain modelling of displacement-field partitioning in transpressional orogens. *Journal of Structural Geology* **16**, 1575–88.

TULLIS, J., CHRISTIE, J. M. & GRIGGS, D. T. 1973. Microstructures and preferred orientations of experimentally deformed quartzites. *Geological Society of America Bulletin* **84**, 297–314.

VANÍČEK, I. & VANÍČEK, M. 2008. *Earth Structures in Transport, Water and Environmental Engineering*. Dordrecht: Springer, 637 pp.

VERGÉS, J., SAURA, E., CASCIELLO, E., FERNÁNDEZ, M., VILLASEÑOR, A., JIMÉNEZ-MUNT, I. & GARCÍA-CASTELLANOS, D. 2011. Crustal-scale cross-section across the NW Zagros Belt: implications for the Arabian Margin reconstruction. *Geological Magazine* **148**, 739–76.

VERNANT, P., NILFOROUSHAN, F., HAZTFELD, D., ABASSI, M., VIGNY, C., MASSON, F., NANKALI, H., MARTINOD, J., ASHTIANY, A., BAYER, R., TAVAKOLI, F. & CHÉRY, J. 2004. Contemporary crustal deformation and plate kinematics in Middle East constrained by GPS measurement in Iran and northern Oman. *Geophysical Journal International* **157**, 381–98.

WALLIS, S. R. 1992. Vorticity analysis in a metachert from the Sanbagawa Belt, SW Japan. *Journal of Structural Geology* **14**, 271–80.

WALLIS, S. R. 1995. Vorticity analysis and recognition of ductile extension in the Sambagawa belt, SW Japan. *Journal of Structural Geology* **17**, 1077–93.

XYPOLIAS, P. 2009. Some new aspects of kinematic vorticity analysis in naturally deformed quartzites. *Journal of Structural Geology* **31**, 3–10.

XYPOLIAS, P. & DOUTSOS, T. 2000. Kinematics of rock flow in a crustal-scale shear zone: implication for the orogenic evolution of the southwestern Hellenides. *Geological Magazine* **137**, 81–96.

https://doi.org/10.1017/S0016756816000558 Published online by Cambridge University Press